A Fresh Perspective on the Photophysics of Benzophenone

Andrew Monkman

a.p.monkman@durham.ac.uk

Durham University https://orcid.org/0000-0002-0784-8640

Carolina Francener

Durham University

Hector Miranda-Salinas

Durham University https://orcid.org/0000-0001-6403-5251

Larrisa Gomes Franca

Department of Materials Science and Metallurgy University of Cambridge

Article

Keywords:

Posted Date: September 29th, 2025

DOI: https://doi.org/10.21203/rs.3.rs-7536619/v1

Additional Declarations: There is **NO** Competing Interest.

A Fresh Perspective on the Photophysics of Benzophenone

Carolina Francener, Hector Miranda-Salinas, Larissa Gomes Franca and Andrew Monkman

C. Francener, H. Miranda-Salinas, L.G. Franca, A. Monkman

Organic Electroactive Materials Research Group, Physics Department, Durham University DH1 3LE, United Kingdom.

L.G. Franca

Department of Materials Science and Metallurgy, University of Cambridge, CB3 0FS, United Kingdom.

ABSTRACT

Aromatic ketones, such as benzophenone (**BP**), are widely used as photophores and triplet sensitizers in photochemical reactions. It is also employed in donor-acceptor delayed fluorescence systems. **BP** is the benchmark for studying the photophysics of aromatic ketones due to its efficient triplet generation. Despite its importance, many spectroscopic properties of **BP** have not been critically investigated in recent times. Here we report the characterization of **BP** using steady-state and time-resolved optical techniques in non-polar environments. The planar structural analogue, 10,10-dimethylanthrone (**DMA**), was also studied to assess the degree of importance that the **BP** molecular structure plays. Both **BP** and **DMA** exhibit direct triplet absorption and instantaneous phosphorescence, challenging current models of fast triplet formation in ketones. Surprisingly, high-energy excitation produces anti-Kasha S_2 emission alongside S_1. The intersystem crossing (ISC) mechanism was further clarified through transient absorption measurements. This work offers fresh insights into aromatic ketone photophysics.

MAIN

Introduction

Aryl ketones play a relevant role in synthetic chemistry, primarily as efficient photosensitizers [1–4]. They readily form triplets upon photoexcitation with ultraviolet radiation, which can be transferred to organic substrates and lead to subsequent reactions [5]. Aryl ketones act as intermediators of synthetic transformations. They enable hydrogen atom transfer (HAT)[6,7] and H-abstraction from a wide range of organic functional groups [8–10], opening the doors for novel synthetic routes. More recently, aromatic ketones have been used as an acceptor unit in materials with delayed fluorescence[11,12] for optical applications, such as organic light-emitting diodes (OLEDs)[13–15], and sensitizers for the up-conversion of solar radiation to the UV[16] displaying another side its versatile application in the field of photonics. Within this scope, benzophenone (BP) is the simplest example of an aryl ketone and is often utilized as a model molecule to probe their excited state dynamics, triplet-state formation and reactivity [17–19].

The properties of **BP**, and other aryl ketones, arises from the high population of triplet states that are photogenerated and effectively transferred[20–22]. The efficiency of intersystem crossing (ISC) from the singlet (S) to triplet (T) manifold is close to unit [23,24] and the reported values of the ISC rate (k_{ISC}) in solution range from 2 to 30 ps^{-1}, depending on the polarity of the environment [25,26]. Given that **BP** is a purely organic molecule, these values appear unusually large considering that, in theory, both S_1 and T_1

states would have a nπ* character, making such transition forbidden by El-Sayed's rule[27]. However, it has been proposed that the twisted structure of **BP** causes the T_1 state to acquire a mixed $^3\pi\pi^*/^3n\pi^*$ character [28,29], explaining the fast process that is experimentally observed. However, efficient ISC has been reported for anthrone, a planar aryl ketone with pure $n\pi^*$ character for S_1 and T_1 states [30,31]. The mechanistic pathway for triplet formation in **BP** remains a topic of ongoing debate [19,32]. While some evidence supports a direct $S_1 \rightarrow T_1$ transition [33], most studies in recent literature suggest the involvement of a higher-lying triplet state T_2 ($S_1 \rightarrow T_2 \rightarrow T_1$) [18,34,35].

Despite the relevance of benzophenone, much of its foundational data stems from work conducted decades ago [36]. In this study, we explore the photophysics of benzophenone in solid and fluid non-polar environments through state-of-the-art steady-state and time-resolved techniques. To isolate the effect of the molecular twist on ISC efficiency, we further examine 10,10-dimethylanthrone (**DMA**), a structurally analogous but planar aryl ketone. By comparing **BP** and **DMA**, we aim to unify the understanding of the photophysics and structure–property relationships governing ISC in aromatic ketones.

RESULTS AND DISCUSSION

Optical properties

The optical properties of **BP** and **DMA** (Fig. 1a) were studied in zeonex (a branched polyolefin used in the manufacture of compact discs) host-guest films at 1% wt/wt concentrations (Fig. 1). Room temperature (RT) steady-state (SS) photoluminescence (PL) (Fig. 1b and d) shows a strong dependence of emission with excitation energy, with a steady red shift of emission spectra when the samples are excited with progressively lower energy. Excitation with wavelengths lower than 300 nm were avoided due to matrix absorption. The films were further measured at 80 K to improve spectral resolution (Fig. 1c and e). In the frozen matrix, we observe two separate emissions in both molecules: denoted I and III. Both vibrationally well resolved bands with onsets at 350 nm and 400 nm. The phosphorescence emission from **BP** has often been reported in the literature as a well-resolved curve with 400 nm on-set[37,38]. The same signal was identified in our measurements of **BP** (Fig. 1c – 3.4 eV excitation). **DMA** presents emission at the same wavelengths but with more resolved vibronic structure at RT (Fig. 1e – 3.5 eV excitation). Therefore, I and III are, respectively, assigned as fluorescence and phosphorescence. Emission from an aggregate state was also identified under lower-energy excitation (<3.3 eV, 375 nm) (Supplementary Fig. 1). Time-resolved photoluminescence (TRPL) experiments were also performed (Fig. 1f and g and Supplementary Fig. 2). At RT, **BP** and **DMA** emission undergoes an apparent red shift in the first 20 ns as singlet emission decays and phosphorescence becomes more predominant. Weak phosphorescence is observable until 120 and 200 μs for **BP** and **DMA**, respectively. Phosphorescence is far stronger at 80 K; therefore, no red shift is observed in the early times as the signal is strong. However, the spectra delayed by 1.1 ns are very broad, ascribed to emission from hot vibrational states. An emission feature at 375 nm with a fast decay is observed, hinting at a contribution from a further singlet state, which has low intensity compared to the phosphorescence. Notably, pure phosphorescence is observed from delay times as short as 9 ns and 12 ns for **BP** and **DMA**, respectively. Considering how predominant the phosphorescence is in the radiative decay, cyclooctatetraene (COT), a triplet excited state quencher [39], was doped into the host-guest films, and the photophysical properties remeasured at room temperature. The resulting PL spectra (Fig. 2 a and b) and TRPL measurements (Fig. 2 c and d) show complete quenching of the phosphorescence. Moreover, an emission that was, seemingly, not seen in the pure films is observed between 355 nm and 600 nm, under a wide range of excitation energies - 3.4 eV to 3.9 eV - (denoted as II). Analyzing the PL spectra of **DMA**:zeonex at RT (Fig. 1d), it is possible to identify isolated emission II with 3.5 eV excitation. Picosecond time-

correlated single photon counting (Ps-TCSPC) was used to acquire the lifetimes of bands I and II to correctly attribute them (Fig. 2g and h and Supplementary Fig 3 and Table 1). Decay II has a decay time of 403 ps and 339 ps for **BP** and **DMA**, respectively, I in **DMA** has a lifetime of 38 ps. The respective emission decay could not be measured accurately in **BP** as it was faster than the system's internal response function (IRF-15 ps). Considering their lifetimes and energies, II is attributed to prompt fluorescence (PF) from the S_1 state, whereas I is anti-Kasha PF from the S_2 state. Such S_2 emission has been reported in a small number of other molecules such as azulene[40], anthraquinone[41] and xanthione[42]; this is an indication that both ISC from S_2 to the triplet manifold, and internal conversion (IC) from S_2 to S_1 in **BP** and **DMA** are slow enough to allow radiative decay to compete with them. Typically, to see emission, radiative decay rates need to be no less than 10^3 smaller than both ISC and IC rates[43]. S_2 emission with low intensity can be seen in **DMA** films, exciting at 300 and 320 nm, but is difficult to observe in the presence of COT due to an overlap of the tail of COT absorption and with S_2 emission between 350 nm and 400 nm (Supplementary Fig. 4). The Stokes shift between S_0-S_1 absorption and S_1-S_0 emission are thus 0.33 eV and 0.12 eV for **BP** and **DMA**, respectively. S_2 Stokes shifts are larger, at 0.42 eV and 0.29 eV, respectively. We ascribe this energy relaxation to changes in the twist dihedral angle about the C=O bond in the triplet excited state for **BP**. **DMA** undergoes less vibrational relaxation in the excited state and exhibits increased vibrational resolution of its emission when compared to **BP**, due to its increased molecular rigidity. A comprehensive PL spectrum with the decays from S_2, S_1 and T_1 is given in Fig. 2h and g. Singlet emission decays from zeonex films, obtained with ps-TCSPC (Fig. 2g and f), also showed a second (relatively long) component, with lifetime of 1.8 ns and 2.5 ns for **BP** and **DMA**, respectively. This second component indicates the presence of a delayed fluorescence (DF) and is corroborated by the decay of **BP** in solution in the ns region in the presence and absence of COT, discussed below. (Supplementary Fig. 5). The observed lifetime of 3.2 ns was reduced to 1.9 ns when COT was added to the solution as the triplets giving rise to the DF were quenched. Not all DF is quenched by COT because the radiative singlet decay is in competition with the diffusion rate of the COT molecules in solution. We believe that the DF is generated whilst the excited states cool through vibrational relaxation and so may indicate the DF coming from T_2 to S_1 and as the T_2 population rapidly decays down to T_1 (see latter section) the DF is rapidly quenched. The emission of single crystals of **BP** and **DMA** was also measured (Supplementary Fig. 6). Only phosphorescence is observed in this case, indicating very rapid quenching of the singlet states. **DMA** presents two distinct phosphorescence bands (Supplementary Fig. 7), ascribed to phosphorescence from two distinct molecular packing motifs in the crystal structure (Supplementary Fig. 8)

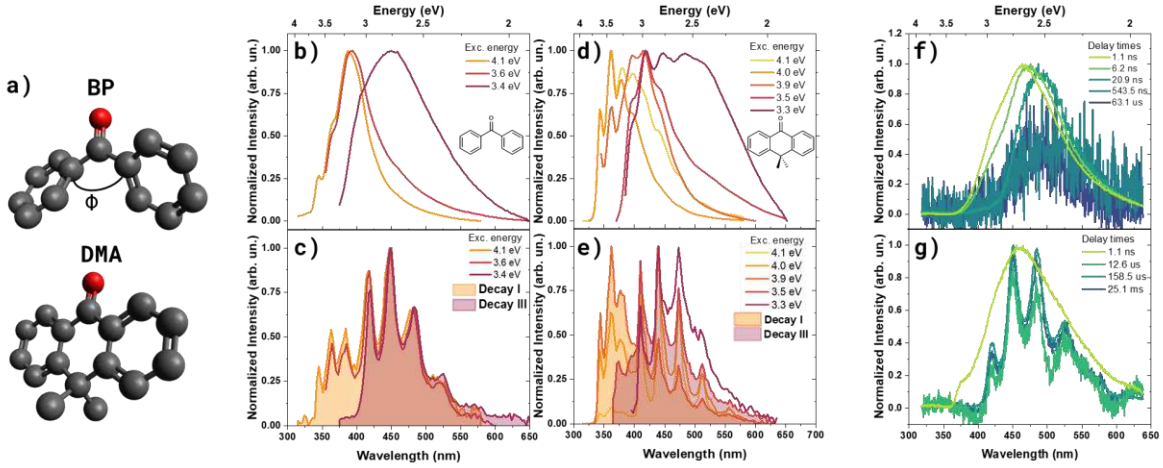

Fig 1. Steady-state and time-resolved spectroscopy of the investigated molecules. Molecular structure of **BP** and **DMA**. Dihedral angle (Φ) of **BP** ranges between 30° to 65° depending on the environment [44,45] (**a**). Normalized steady-state of **BP** (**b**,**c**) and **DMA** (**d**,**e**) in a host-guest film with Zeonex as polymeric matrix (1% wt/wt) under varied excitation energies at room temperature (**b**,**d**. Top panel) and 80 K (**c**,**e**. Bottom panel). Decays I and III are identified in low temperature plots for both emitters. Normalized time-resolved emission spectra of **BP** at room temperature (**f**) and 80 K (**g**). $\lambda_{exc} = 355\ nm$.

The photophysical behavior of **BP** and **DMA** was also evaluated in solution state. Absorption in methylcyclohexane (MCH) 20 µM solution are in Supplementary Fig. 9. Absorbance was also recorded varying the concentration of **BP** in MCH (Supplementary Fig. 10). An increase from 10 µM to 20 µM was sufficient to quench some of the absorption intensity, indicating a formation of aggregates even at this low concentration. The emission of ketones was also evaluated in solvents with varying polarity. From Supplementary Fig. 11a and b, it is observed that, in aerated and degassed solutions, only S_2 emission is observed, and its intensity is only slightly enhanced by removing oxygen and no significant shifts are observed when the polarity of the medium was changed. Since benzophenone is known to undergo H-abstraction reactions in the excited state, the emission was measured in tetrachloromethane (CCl_4) (Supplementary Fig. 11c). In this case, intense phosphorescence from **BP** was observed in a room temperature, non-degassed solution of CCl_4 under various excitation energies. The observation of solution state room temperature phosphorescence (sRTP) only in non-hydrogenated solvents makes it clear how aryl ketone's behavior is critically dependent on the environment and how reactive they become in the (triplet) excited state.

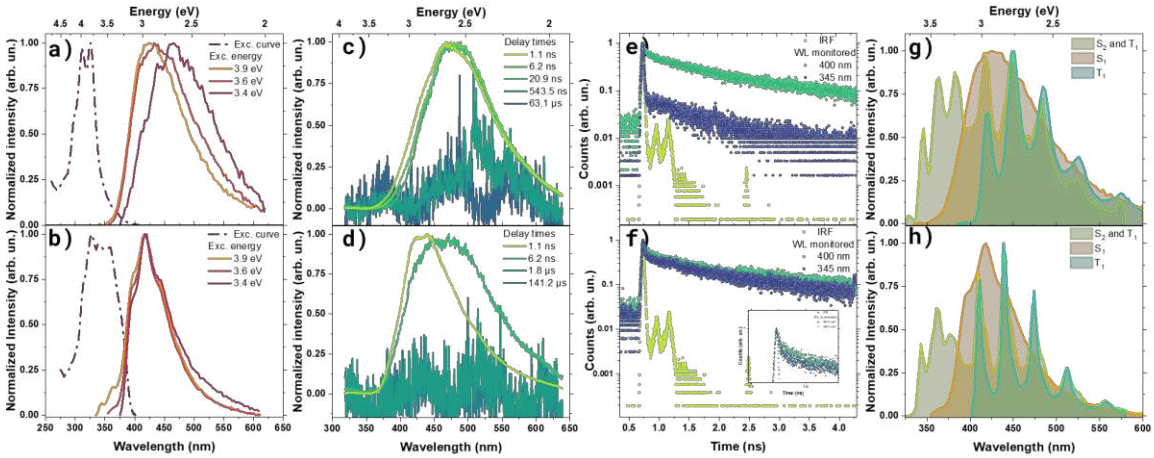

Fig 2. Photophysical measurements employing triplet quencher and decay assignment. Normalized steady-state of **BP** (**a**) and **DMA** (**b**) in a host-guest film with Zeonex as polymeric matrix (1% wt/wt) doped with cyclooctatetraene (COT) (10% wt/wt) under varied excitation energies. Aggregate emission is observed from **BP** under 3.4 eV excitation. Normalized time-resolved emission spectra of **BP** (**c**) and **DMA** (**d**). $\lambda_{exc} = 355\ nm$. Picosecond time-correlated single photon counter decay curve of **BP** (**e**) and **DMA** (**f**) Beam reflection is observed on IRF decay profile. Decay collected at 400 nm employed host-guest films doped with COT (10% wt/wt) to collect emission coming from S_1 state. Here $\lambda_{exc} = 323\ nm$. Bi-exponential fitting yield decay lifetimes of 403 ps and 1.8 ns for **BP** and 339 ps and 2.5 ns for **DMA**. Decay collected at 345 nm was employed to collect emission coming from S_2 state. Here $\lambda_{exc} = 309\ nm$. Bi-exponential fitting yield decay lifetimes of 13 ps (assigned to IRF) and 0.9 ns for **BP** and 38 ps and 1.1 ns for **DMA**. Reflection on the quartz substrate caused additional peaks in the IRF signal. PL curves of the host-guest films attributed to S_2, S_1 and T_1 states for **BP** (**g**) and **DMA** (**h**). S_2 emission was collected at 80 K under 4.1 eV excitation. S_1 at room temperature under 3.6 eV excitation in the presence of COT. T_1 at 80 K under 3.5 eV excitation.

Observation of direct triplet absorption

Phosphorescence is observed with excitation energies of 3.26 eV (380 nm) for **BP** and 3.18 eV (390 nm) for **DMA**. These energies sit well below the S_1 state for both molecules. This could be ascribed to excitation of Boltzmann thermally populated vibronic states of the electronic ground state, S_0, however we observe the same at low temperatures. It can thus be ascribed to direct excitation from S_0 into the triplet manifold. Therefore, excitation was monitored for **BP**, in the presence and absence of the triplet quencher (Fig 3a and b). $S_0 \rightarrow S_1$ excitation curve was determined from the sample with COT, where only S_1 PF is observed, independent of excitation energy. However, upon examining the excitation spectrum of the film without COT and monitoring the phosphorescence emission at 448 nm, it shows that there is a structured absorption band that sits at lower energy compared to the S_1 absorption band that generates phosphorescence. This is attributed to the spin-forbidden direct $S_0 \rightarrow T_1$ absorption. This band has previously been attributed to a singlet $n\pi \rightarrow \pi\pi^*$ transition[46,47]. When this excitation band is compared to that of the phosphorescence, there is a close resemblance, but not a perfect mirror image which we conclude arises from the overlap of absorption from S_0 to the close by T_2 state (Fig 3c and d). Calculations indicate T_1 and T_2 to be only 0.08 eV apart[35]. Direct triplet absorption is also visible in the excitation profile of **DMA** (Supplementary Fig. 12, below 4 eV); however, the intensity is weaker compared to **BP** since the T_1 state in **DMA** has a pure $n\pi^*$ character, reducing the oscillator strength of the direct transition. The $S_0 \rightarrow T_1$ transition is also observed in solution absorption measurements with extinction coefficients of 72.8 $M^{-1}cm^{-1}$ and 80.1 $M^{-1}cm^{-1}$ for **BP** and **DMA**, respectively (Supplementary Fig 9). Any Contribution from $S_0 \rightarrow T_1$ transition to triplet formation is hidden under the $S_0 \rightarrow S_2$ and $S_0 \rightarrow T_1$ bands due to the low oscillator strength of the $S_0 \rightarrow S_1$ $n\pi^*$ absorption (Fig. 3b – monitored at 448 nm). From Fig. 3b it is noticeable that excitation into the S_2 state is also an effective route for phosphorescence, therefore, along with weak anti-Kasha emission from S_2, S_2 decays non-radiatively to T_N via ISC. On the other hand, S_2 excitation does not seem to lead to S_1 prompt fluorescence, indicating that there is little S_2 to S_1 IC indicating weak coupling between the S_2 $\pi\pi^*$ state and the $n\pi^*$ S_1 state. As the direct instantaneous population of triplet states is possible and achievable with a wide range of excitation energies, experimental determination of ISC rates need to be carefully conducted, given that over estimation can easily be achieved through inadvertent inclusion of direct T_1 excitation.

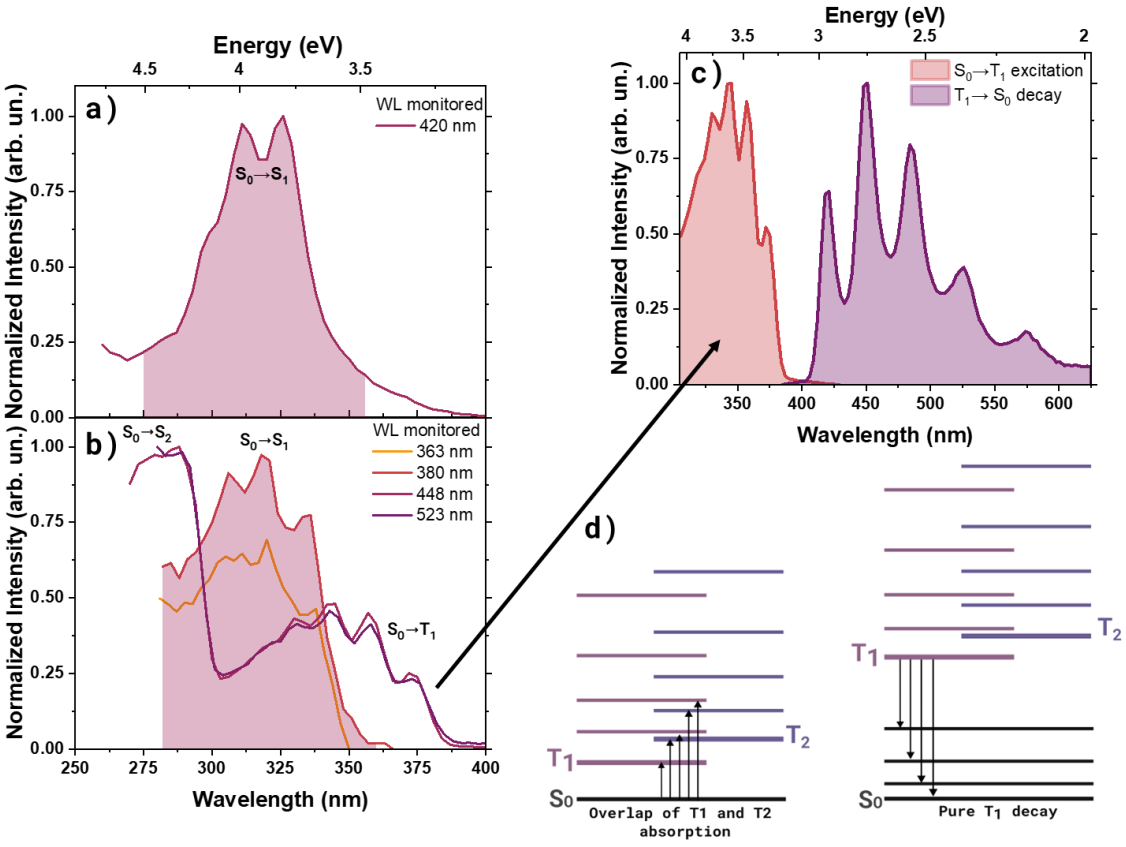

Fig 3. Investigation of direct $S_0 \rightarrow T_1$ absorption. Excitation profile for $S_0 \rightarrow S_1$ transition in **BP**; obtained from host-guest film doped with cyclooctatetraene (COT) (10% wt/wt). Emission was monitored at 420 nm. This is attributed to $S_0 \rightarrow S_1$ transition since S_1 decay is the only emission observed from the films with the triplet quencher (**a**) Excitation curves of $S_0 \rightarrow S_2$, $S_0 \rightarrow S_1$ and $S_0 \rightarrow T_1$ transitions for **BP**; obtained from host-guest films (**b**) $S_0 \rightarrow T_1$ excitation and $T_1 \rightarrow S_0$ decay curves for **BP**; obtained from host-guest film (**c**) Diagram displaying the overlap of the triplet states T_1 and T_2, clarifying the shape of the $S_0 \rightarrow T_1$ excitation curve (**d**) All measurements were carried out using zeonex polymeric matrix doped with **BP** at 1% wt/wt.

Transient absorption spectroscopy

The measured excited state induced absorption (ESA) for both **BP** and **DMA** in toluene, excitation at 343 nm, are shown in Fig. 4. In both cases we observe near instantaneous grow in of ESA at 470 nm which also decays rapidly within 2 ps. Along with this fast species we observe the grow-in of a band centered around 540 nm which lives beyond our measurement time window of 6 ns. Clearly this is the ESA from the lowest triplet state of both **BP** and **DMA**. From the plots of the ESA intensity at 560 nm we observe an initial near instantaneous population formed within the first 2 ps then a slower grow in over 30 ps. The fast component matches the decay of the fast ESA feature at 470 nm. Thus, we ascribe the initial fast population of the T_1 state being formed through the T_2 state, itself populated rapidly by ISC from S_1. The slow component we ascribe to T_1 population directly from the S_1 state. Within our spectral window we do not observe an ESA feature associated with the S_1 state, however we do observe S_1 emission when exciting at 340 nm indicating that 343 nm excitation must create S_1 population (Fig 2a and b). We cannot rule out some direct excitation of T_2 through direct S_0-T_2 absorption, however. From the theoretical calculations of Marian et al[28], in the case of **BP**, T_2 lies at slightly higher energy than S_1 but excitation at 343 nm can excite S_1 into a vibrationally excited state which we believe will enable rapid initial ISC from S_1* to T_2. As S_1^* rapidly thermalizes then ISC to T_2 becomes endothermic, potentially reducing the ISC rate below that of direct ISC from S_1 to T_1, hence the T_2 population is

rapidly quenched and the thermalized S_1 states populates T_1 directly via ISC throughout the singlet lifetime. Non-thermalized initial triplet states are in accordance with the structureless triplet emission observed during the first ns after excitation, indicating the presence of hot excited (singlet and triplet) states[48] (Fig. 1g) and agrees with the model proposed by Hochstrasser et al[36]. From our measured T_1 ESA build in times for **BP** ca. 30 ps and **DMA** ca 17 ps, Supplementary Fig. 13 and 14, we conclude that ISC S_1-T_1 is faster in **DMA** which indicates a better alignment of S_1, T_1 and T_2 for ISC in **DMA.** From the measured (slow) T_1 build-up it is possible to extract the k_{ISC}: 2.9×10^{10} s^{-1} and 5.4×10^{10} s^{-1}, for **BP** and **DMA**, respectively, in a low polarity environment. **BP's** ISC is up to 3-times slower than previously reported and often attributed to ISC S1-T2[26,49,50]. $S_1 \rightarrow T_2$ k_{ISC} is in sub-ps range and could not be fitted, however this process may also be quenched via thermalization of S_1 and so may not be truly representative of the true rate. The experimental k_{ISC} represent the average of the calculated rates between $S_1 \rightarrow T_1$ and $S_1 \rightarrow T_2$ [28], which further corroborates dual intersystem crossing pathways. A further weak ESA band is observed centered at 720 nm. From the decay kinetics we again observe instantaneous formation, a 2 ps decay component then a constant ESA beyond 6 ns. This behavior again matches the decay kinetics of both T_2 and T_1 populations with strongly overlapping ESA spectra as they are energetically very close. Given that T_2 and T_1 are so close in energy we can assume that they both could be excited to the same upper T_N state so their ESA overlap. As **DMA** gives very similar ESA features and decay kinetics, we believe that in toluene the T_2 state in **DMA** also lies slightly higher in energy than S_1. No S_2 states can be generated with excitation at 343 nm. We point out that we made every effort to make these measurements at lowest possible concentration to avoid aggregation effects and used an excitation wavelength that we know directly photocreates S_1 excited states in both **BP** and **DMA**, (through the observation of S_1 fluorescence at this excitation wavelength) even in the presence of a triplet quencher. The energetic proximity between T_1 and T_2 indicates that as the solvent environment changes to higher polarity then energetics of the states will change, changing the dynamics of ISC and changing the relative dynamics between **BP** and **DMA** given the mixed character of the **BP** states compared to pure n and π character of the states in **DMA**[26]. This we believe is the reason for many differences in the reported photophysics of **BP** in literature.

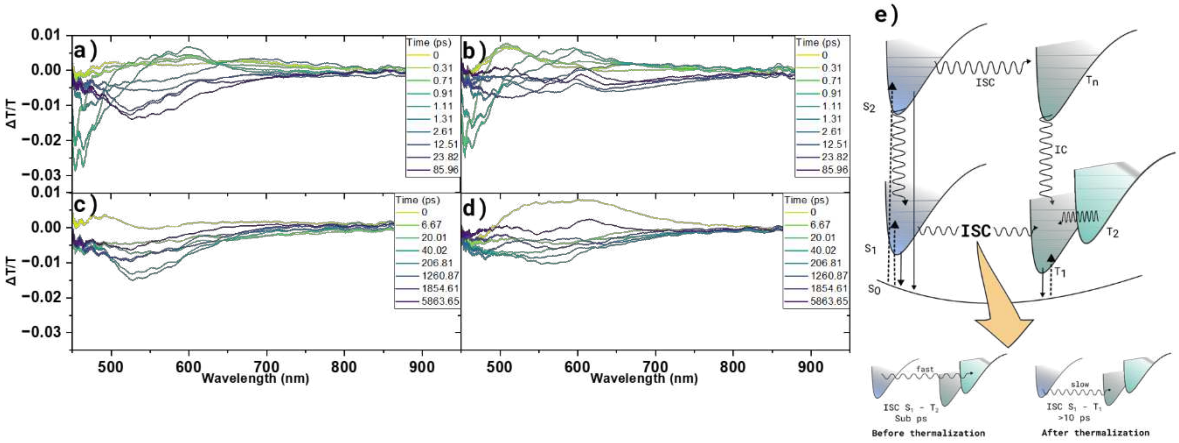

Fig 4. Early time evolution of excited state absorption and ISC mechanism evaluation. Transient absorption in the probe window from 460 nm to 950 nm and in the time window of ps and ns for **BP** (**a**, **c**) and **DMA** (**c**, **d**). [c] = 2×10^{-3} M in degassed toluene solution. $\lambda_{exc} = 343\ nm$. Diagram displaying the general electronic properties of both **BP** and **DMA** and illustration of the ISC mechanism. Absorption, non-radiative decays and radiative decays are indicated by dashed, wavy and solid arrows, respectively.

Electronic structure of BP and DMA

Based on the data collected from our experiments, it is possible to energetically position the electronic states of **BP** and **DMA**, as well as their electronic mechanisms, in non-polar environments, as shown in the diagram in Fig. 4e and 5a and b. Their decay pathways have proven to be highly dependent on excitation energy. To recapitulate, high energies (> 3.65 eV) populate the S_2 state, which decays in competition between ISC to T_N and radiative decay to S_0. The observation of anti-Kasha emission indicates a decoupling between a S_1 $n\pi^*$ and S_2 $\pi\pi^*$ states. When excited into S_1, electrons can promptly decay to the ground state or competitively ISC to T_2 then T_1 as the S_1 state thermalizes. A direct pathway from S_0 to T_1 is also possible for the molecules, allowing for instantaneous triplet state population and fast phosphorescence decay, in the range of sub-nanoseconds potentially. Similar photophysical behavior was observed for **BP** and **DMA**, indicating little direct effect attributed to the lack of molecular torsion in **DMA**. This only results in the mixing of the $n\pi^*$ and $\pi\pi^*$ character of the triplet states in **BP**. Notably, in non-polar environments the planar structure of **DMA** led to a 2-fold increase in the ISC rate. The twist in **BP** has a minor direct effect on ISC but does change the relative energy separations of S_1 T_2 and T_1 which has a far greater effect on ISC rates.

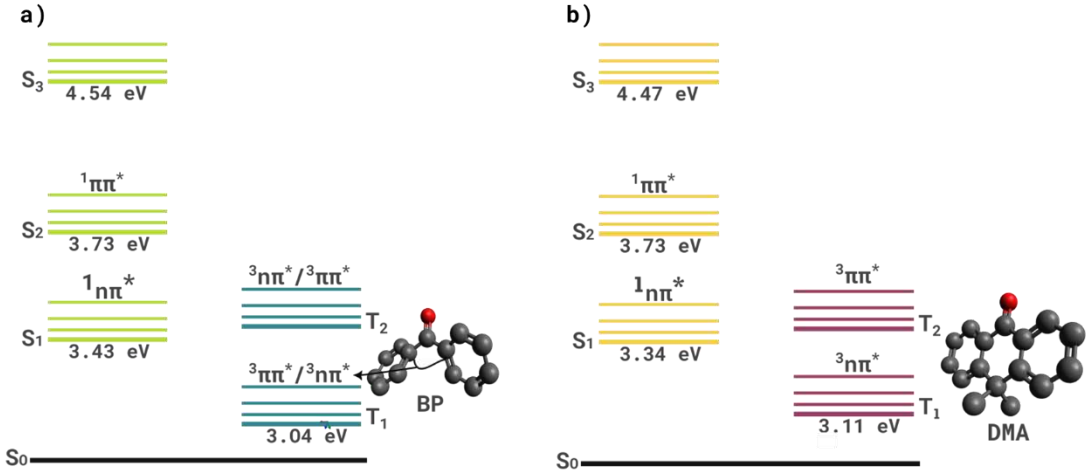

Fig 5. Energy levels of BP and DMA in non-polar environments. Diagram of the excited states of **BP** (**a**) and **DMA** (**b**) illustrate the character and energy of each state.

To conclude, the photophysical properties of **BP** were re-examined along with its planar analog **DMA**, via a thorough analysis of steady state and time-resolved photophysics. They reveal emissions from S_2, S_1 and T_1 states, with notable direct T_N absorption. The excitation spectra of the transitions were also characterized. From our photoinduced absorption measurements, in non-polar solvents, we conclude that S_1 lies energetically slightly below T_2 in both **BP** and **DMA** and ISC proceeds first through $S_1^* \rightarrow T_2$ crossing but, as S_1^* thermalizes, this channel becomes too endothermic and ISC $S_1 \rightarrow T_1$ takes over. Thus, both T_2 and T_1 are involved in ISC but not sequentially, rather in dynamic competition with S_1 thermalization driving the competition. **BP** and **DMA** presented similar photophysical behavior of their excited states, apart from slight changes to the lifetime of both radiative and non-radiative processes, mainly caused by the fact that **BP** has triplet orbitals with mixed $n\pi^*$ and $\pi\pi^*$ characters due to its twisted structure, as opposed to **DMA**'s planar geometry. Overall, these findings help clarify the non-conventional processes that aryl ketones undergo in the excited state and shine light on the complexities of their photophysics, especially the complex excitation dependent properties of these molecules and the care required to avoid aggregation. These new results will be invaluable considering the important role this class of molecules plays in a plethora of applications in the field of organic and material

chemistry. As a simple example, ketocoumarins have been shown to be excellent triplet sensitizers in visible to UV solar up-conversion [51], however the twisted substituted **BP** like molecules used are not stable and tend to cleave at the central keto group, but from our new results this problem can be solved by going over to a central **DMA** structure which will not affect the efficiency of triplet formation. This work shows the value that can be gained by going back to reexam key photophysical and photochemical mechanisms that have simply been accepted for decades in many cases, there is much new information waiting to be uncovered.

METHODS

Steady State Measurements

Absorption, photoluminescence, and excitation measurements were obtained using drop-cast films on sapphire substrates at 1% by weight for zeonex (1 wt. %); for the solution measurement, concentrations ranging from 10 20 μM L^{-1} to 100 μM L^{-1} were used. Solutions were dissolved by bubbling with argon. A (double-double) spectrofluorometer (Jobin Yvon Horiba Fluorolog) and a spectrophotometer (Shimadzu UV–vis–NIR 3600) were used for emission and absorption measurements, respectively. For vacuum and/or cryogenic temperature measurements the samples were placed in a cryostat (Janis Research VNF-100) and cooled down by nitrogen flow. A helium-closed cycle cryopump was used for measurements at 20 K. All spectral onset energies were corrected using the Jacobian conversion of wavelengths to energies.

Time-resolved measurements

The time-resolved measurements were obtained using a gated iCCD camera (250–950 nm) (Stanford Computer Optics 4Picos) with sub-nanosecond resolution and spectrograph equipped with 300 lines/mm grating, 500 nm blaze wavelength system. Excitation was from the 3rd or 4th harmonic of a 200 ps Nd:YAG 10 Hz repetition rate laser (EKSPLA). Time-resolved measurements were made using a variable CCD gate and delay times relative to the laser trigger, allowing emission decays to be constructed from the changes in spectrum area (normalized by gate time). TCSPC measurements were recorded with a double subtractive monochromator (Acton Research Corporation), coupled to a microchannel plate photomultiplier tube (Hamamatsu) and signal was acquired using a TCSPC module (Becker & Hickl) system IRF=15 ps. Samples were excited with the 3rd harmonic generated from a Coherent ps-Ti:saphire laser.

Transient absorption spectroscopy

The laser used in the transient absorption setup is PHAROS from Light Conversion (wavelength: 1030 nm, pulse duration: 180 fs, pulse energy: 0.6 mJ, repetition rate: 1 KHz). Part of the output is used to do third harmonic generation (THG), which produces 343 nm output. We use this 343 nm output to pump our samples and the pulse energy used is about 1 μJ. Another part of the output is used to pump a calcium fluoride disk on a rotating stage to generate white light continuum (WLC). We use this WLC to probe the dynamics of the excited states. The polarization of the pump is vertical to the optical table, while the polarization of the probe is parallel to the optical table. The spot sizes (FW @ $1/e^2$) of the pump and probe are 270 μm and 200 μm, respectively. The time delay between pump and probe is controlled by a 1-meter motorized translation stage (Zaber Technologies Inc. A-LST1000AKT07G06SU), which can generate about 6 ns delay range. The pump is modulated by an optical chopper (Thorlabs Inc. MC2000B-EC) that is locked to the half frequency of the laser repetition rate to create an iterated pump on / pump off situation. The WLC goes through a spectrometer and the intensities at different wavelengths are monitored by a camera (Imaging Solutions Group LightWise

LW-ELIS-1024A-1394). The camera is synchronized with the laser pulse to ensure it captures the spectrum of WLC pulse by pulse. The transient absorption spectrum at one fixed time delay is calculated by

$$\frac{\Delta T}{T} = \left\{ \sum_{i=1}^{N} \frac{Spectrum_{pumpon} - Spectrum_{pumpoff}}{Spectrum_{pumpoff}} \right\} / N$$

where N is average number, in our case N=500. By changing the time delay between pump and probe, we obtain the whole transient absorption spectra.

REFERENCES

1. Großkopf, J., Kratz, T., Rigotti, T. & Bach, T. Enantioselective Photochemical Reactions Enabled by Triplet Energy Transfer. *Chem Rev* **122**, 1626–1653 (2022).
2. Liu, M. *et al.* Blending Aryl Ketone in Covalent Organic Frameworks to Promote Photoinduced Electron Transfer. *J Am Chem Soc* **145**, 9198–9206 (2023).
3. Kamijo, S. *et al.* Aryl Ketone-Catalyzed Light-Driven Radical Oxy-Functionalization of Non-Acidic C(sp^3)−H Bonds Enabled by Triple Role of TEMPO. *Adv Synth Catal* **366**, 1375–1381 (2024).
4. Wu, K. *et al.* Recent progress in triplet energy transfer systems toward organic afterglow materials. *Commun Chem* **8**, 85 (2025).
5. Dumont, E. *et al.* Resolving the benzophenone DNA-photosensitization mechanism at QM/MM level. *Journal of Physical Chemistry Letters* **6**, 576–580 (2015).
6. Luridiana, A. *et al.* The Merger of Benzophenone HAT Photocatalysis and Silyl Radical-Induced XAT Enables Both Nickel-Catalyzed Cross-Electrophile Coupling and 1,2-Dicarbofunctionalization of Olefins. *ACS Catal* **12**, 11216–11225 (2022).
7. Dewanji, A., Krach, P. E. & Rueping, M. The Dual Role of Benzophenone in Visible-Light/Nickel Photoredox-Catalyzed C−H Arylations: Hydrogen-Atom Transfer and Energy Transfer. *Angewandte Chemie International Edition* **58**, 3566–3570 (2019).
8. Dormán, G., Nakamura, H., Pulsipher, A. & Prestwich, G. D. The Life of Pi Star: Exploring the Exciting and Forbidden Worlds of the Benzophenone Photophore. *Chem Rev* **116**, 15284–15398 (2016).
9. Leigh, W. J., Lathioor, E. C. & St. Pierre, M. J. Photoinduced Hydrogen Abstraction from Phenols by Aromatic Ketones. A New Mechanism for Hydrogen Abstraction by Carbonyl n,π* and π,π* Triplets. *J Am Chem Soc* **118**, 12339–12348 (1996).
10. Cao, C. *et al.* Wet Photolithography From Hydrogen Abstraction of a Quasi-Orthogonal Aggregation-Induced Emitter. *Advanced Science* **12**, (2025).

11. Luo, A. *et al.* Design of Thermally Activated Delayed Fluorescence Materials: Transition from Carbonyl to Amide-Based Acceptor. *Angewandte Chemie International Edition* **63**, e202411464 (2024).

12. Zhao, S. *et al.* Realization of highly efficient organic emitting diodes using thermally activated delayed fluorescence (TADF) materials with fast reverse intersystem crossing. *J Mater Chem C Mater* **12**, 5856–5863 (2024).

13. Blazevicius, D. & Grigalevicius, S. A Review of Benzophenone-Based Derivatives for Organic Light-Emitting Diodes. *Nanomaterials* **14**, 356 (2024).

14. Wang, L., Ge, Z., Xu, L. & Song, Y. An effective method in modulating thermally activated delayed fluorescence (TADF) emitters from green to blue emission: the role of the phenyl ring. *Physical Chemistry Chemical Physics* **26**, 5597–5606 (2024).

15. Blazevicius, D. & Grigalevicius, S. A Review of Benzophenone-Based Derivatives for Organic Light-Emitting Diodes. *Nanomaterials 2024, Vol. 14, Page 356* **14**, 356 (2024).

16. Harada, N., Sasaki, Y., Hosoyamada, M., Kimizuka, N. & Yanai, N. Discovery of Key TIPS-Naphthalene for Efficient Visible-to-UV Photon Upconversion under Sunlight and Room Light**. *Angewandte Chemie International Edition* **60**, 142–147 (2021).

17. Venkatraman, R. K. & Orr-Ewing, A. J. Photochemistry of Benzophenone in Solution: A Tale of Two Different Solvent Environments. *J Am Chem Soc* **141**, 15222–15229 (2019).

18. Venkatraman, R. K., Kayal, S., Barak, A., Orr-Ewing, A. J. & Umapathy, S. Intermolecular Hydrogen Bonding Controlled Intersystem Crossing Rates of Benzophenone. *J Phys Chem Lett* **9**, 1642–1648 (2018).

19. Spighi, G., Gaveau, M.-A., Mestdagh, J.-M., Poisson, L. & Soep, B. Gas phase dynamics of triplet formation in benzophenone. *Phys. Chem. Chem. Phys.* **16**, 9610–9618 (2014).

20. Prentice, C., Martin, A. E., Morrison, J., Smith, A. D. & Zysman-Colman, E. Benzophenone as a cheap and effective photosensitizer for the photocatalytic synthesis of dimethyl cubane-1,4-dicarboxylate. *Org Biomol Chem* **21**, 3307–3310 (2023).

21. Chen, J. *et al.* Photocatalytic α-aminoalkyl radical addition of amines mediated by benzophenone under visible light. *Green Chemistry* **26**, 5471–5476 (2024).

22. Sayes, M., Benoit, G. & Charette, A. B. Borocyclopropanation of Styrenes Mediated by UV-light Under Continuous Flow Conditions. *Angewandte Chemie International Edition* **57**, 13514–13518 (2018).

23. Karak, P. & Chakrabarti, S. The influence of spin–orbit coupling, Duschinsky rotation and displacement vector on the rate of intersystem crossing of benzophenone and its fused analog fluorenone: a time dependent correlation function based approach. *Physical Chemistry Chemical Physics* **22**, 24399–24409 (2020).

24. Xie, Y. *et al.* Triplet-triplet energy transfer between host and guest induced strong phosphorescence in the organic doped system. *Next Materials* **3**, 100087 (2024).

25. Tamai, N., Asahi, T. & Masuhara, H. Intersystem crossing of benzophenone by femtosecond transient grating spectroscopy. *Chem Phys Lett* **198**, 413–418 (1992).

26. Aloïse, S. *et al.* The Benzophenone S_1 (n,π*) → T_1 (n,π*) States Intersystem Crossing Reinvestigated by Ultrafast Absorption Spectroscopy and Multivariate Curve Resolution. *J Phys Chem A* **112**, 224–231 (2008).

27. Wu, B. *et al.* The El-Sayed's rule analogy enables long-lived room temperature phosphorescence in twisted biphenyls. *Cell Rep Phys Sci* **4**, 101245 (2023).

28. Metz, S. & Marian, C. M. Modulation of Intersystem Crossing by Chemical Composition and Solvent Effects: Benzophenone, Anthrone and Fluorenone. *ChemPhotoChem* **6**, (2022).

29. Flores-Larrañaga, R., Castro, M. E., Palma, A. & Melendez, F. J. Theoretical Insights of the Non-Rigid Behavior of Benzophenone by Franck-Condon Factors Approach. *Int J Quantum Chem* **125**, (2025).

30. Kobayashi, T. & Nagakura, S. Picosecond time-resolved spectroscopy and the intersystem crossing rates of anthrone and fluorenone. *Chem Phys Lett* **43**, 429–434 (1976).

31. Scott, G. W. & Talley, L. D. The excited state absorption kinetics of anthrone at 533 nm. *Chem Phys Lett* **52**, 431–435 (1977).

32. Marian, C. M. Understanding and Controlling Intersystem Crossing in Molecules. *Annu Rev Phys Chem* **72**, 617–640 (2021).

33. Favero, L., Granucci, G. & Persico, M. Surface hopping investigation of benzophenone excited state dynamics. *Physical Chemistry Chemical Physics* **18**, 10499–10506 (2016).

34. Marazzi, M. *et al.* Benzophenone Ultrafast Triplet Population: Revisiting the Kinetic Model by Surface-Hopping Dynamics. *J Phys Chem Lett* **7**, 622–626 (2016).

35. Sergentu, D.-C., Maurice, R., Havenith, R. W. A., Broer, R. & Roca-Sanjuán, D. Computational determination of the dominant triplet population mechanism in photoexcited benzophenone. *Phys. Chem. Chem. Phys.* **16**, 25393–25403 (2014).

36. Hochstrasser, R. M., Lutz, H. & Scott, G. W. The Dynamics of Populating The Lowest Triplet State Of Benzophenone Following Singlet Excitation. *Chem Phys Lett* **24**, 162–167 (1974).

37. Sun, Y. P., Sears, D. F. & Saltiel, J. Resolution of benzophenone delayed fluorescence and phosphorescence spectra. evidence of vibrationally unrelaxed prompt benzophenone fluorescence1. *J Am Chem Soc* **111**, 706–711 (1989).

38. Matsui, K., Nozawa, K. & Yoshida, T. Phosphorescence of Benzophenone in Sol–Gel Silica. *Bull Chem Soc Jpn* **72**, 591–596 (1999).

39. Mai, V. T. N. *et al.* Solid cyclooctatetraene-based triplet quencher demonstrating excellent suppression of singlet–triplet annihilation in optical and electrical excitation. *Nat Commun* **11**, 5623 (2020).

40. Dunlop, D., Ludvíková, L., Banerjee, A., Ottosson, H. & Slanina, T. Excited-State (Anti)Aromaticity Explains Why Azulene Disobeys Kasha's Rule. *J Am Chem Soc* **145**, 21569–21575 (2023).

41. Itoh, T., Yamaji, M. & Shizuka, H. Observation of the S2-Emission from 1,4-Anthraquinone. *Chem Lett* **29**, 616–617 (2000).

42. Robert Huber, J. & Mahaney, M. S2 → S0 fluorescence in an aromatic thioketone, xanthione. *Chem Phys Lett* **30**, 410–412 (1975).

43. Dunlop, D., Ludvíková, L., Banerjee, A., Ottosson, H. & Slanina, T. Excited-State (Anti)Aromaticity Explains Why Azulene Disobeys Kasha's Rule. *J Am Chem Soc* **145**, 21569–21575 (2023).

44. Volovšek, V., Baranović, G. & Colombo, L. Vibrational analysis of the benzophenone molecule and influence of its conformation on vibrational transitions. *Spectrochim Acta A* **49**, 2071–2080 (1993).

45. Coppens, P., Ma, B., Gerlits, O., Zhang, Y. & Kulshrestha, P. Crystal engineering, solid state spectroscopy and time-resolved diffraction. *CrystEngComm* **4**, 302–309 (2002).

46. Su, Y. *et al.* Disrupting n-π* Transition of Benzophenone Derivatives' T_1 States to Achieve Ultralong-Lived Room-Temperature Phosphorescence. *ACS Mater Lett* **6**, 1042–1049 (2024).

47. Hochstrasser, R. M. & Noe, L. J. Excited state dipole moments of benzophenone in singlet and triplet n states. *J Mol Spectrosc* **38**, 175–180 (1971).

48. Greene, B. I., Hochstrasser, R. M. & Weisman, R. B. Picosecond transient spectroscopy of molecules in solution. *J Chem Phys* **70**, 1247–1259 (1979).

49. Tamai, N., Asahi, T. & Masuhara, H. Intersystem crossing of benzophenone by femtosecond transient grating spectroscopy. *Chem Phys Lett* **198**, 413–418 (1992).

50. Venkatraman, R. K. & Orr-Ewing, A. J. Photochemistry of Benzophenone in Solution: A Tale of Two Different Solvent Environments. *J Am Chem Soc* **141**, 15222–15229 (2019).

51. Uji, M. *et al.* Heavy metal-free visible-to-UV photon upconversion with over 20% efficiency sensitized by a ketocoumarin derivative. *J Mater Chem C Mater* **10**, 4558–4562 (2022).

Supplementary Files

This is a list of supplementary files associated with this preprint. Click to download.

- BPDMASI.docx